Pt^+-Catalyzed Oxidation of Methane: Theory and Experiment

Maria Pavlov, Margareta R. A. Blomberg, and Per E. M. Siegbahn*

Department of Physics, University of Stockholm, Box 6730, S-113 85 Stockholm, Sweden

Ralf Wesendrup, Christoph Heinemann, and Helmut Schwarz*

Institut für Organische Chemie, Technischen Universität Berlin, Strasse des 17.Juni 135, D-10623 Berlin, Germany

Received: September 26, 1996; In Final Form: December 12, 1996[⊗]

The oxidation of methane with molecular oxygen using the atomic platinum cation as a catalyst, yielding methanol, formaldehyde, and higher oxidation products, has been studied both computationally and experimentally. The most relevant reaction pathways have been followed in detail. To this end a large number of stationary points, both minima and transition states, have been optimized using a hybrid density functional theory method (B3LYP). At these optimized geometries, energies have been calculated using both an empirical scaling scheme (PCI-80) and the B3LYP method employing extended basis sets with several polarization functions. Good agreement with available experimental data has been obtained. For the parts of the catalytic cycle where detailed experimental results have not been available, the new calculated results have complemented the experimental picture to reach an almost complete understanding of the reaction mechanisms. Spin−orbit effects have been incorporated using an empirical approach, which has lead to improved agreement with experiments. The new FTICR experiments reported in the present study have helped to clarify some of the most complicated reaction sequences.

I. Introduction

The transition-metal-mediated functionalization of methane constitutes an important topic of research stimulated by both the challenging inertness of this simplest hydrocarbon molecule and the substantial industrial interest in the use of natural gas resources.[1−5] Not surprisingly, methane activation by transition-metal cations has also been at the focus of a number of fundamental studies in the gas phase.[6−8] Irikura and Beauchamp discovered that "bare" third-row transition metal cations M^+ (M = Ta, W, Os, Ir, Pt) dehydrogenate methane in a stoichiometric manner to yield the corresponding carbene complexes $M(CH_2)^+$.[9−11] The reaction is driven by the formation of the strong metal−methylidene bond (BDE ≥ 111 kcal/mol),[12] and this remarkable bond strength can be attributed to relativistic stabilization of the cationic complexes $M(CH_2)^+$ [13] as demonstrated by fully relativistic four-component Dirac−Fock Coulomb benchmark calculations including correlation effects.[14] The reactions of Ir^+,[15,16] Pt^+,[17] and other transition metal cations M^+ with methane have also formed the subject of detailed theoretical investigations using different levels of theory.[18−21]

Recently, it has been discovered that bare Pt^+ catalyzes the reaction of methane with molecular oxygen in the gas phase, yielding methanol, formaldehyde, and higher oxidation products (see Scheme 1).[22] A key step in the catalytic cycle is the reaction of $Pt(CH_2)^+$ with O_2 to mainly (70%) regenerate Pt^+ via liberation of neutral $[C,H_2,O_2]$ which either represents vibrationally excited formic acid and/or its decomposition products CO/H_2O and CO_2/H_2, respectively. While the actual structure of the emerging neutral(s) cannot be deduced from the experiment, it has been shown in charge-transfer experiments with fluorinated benzenes that Pt^+ is partially formed in its $^4F_{9/2}$ electronic excited state during this oxidation process.[17] To uncover the nature of the neutral products and to gain some insight into mechanistic details of the reaction pathway,

SCHEME 1

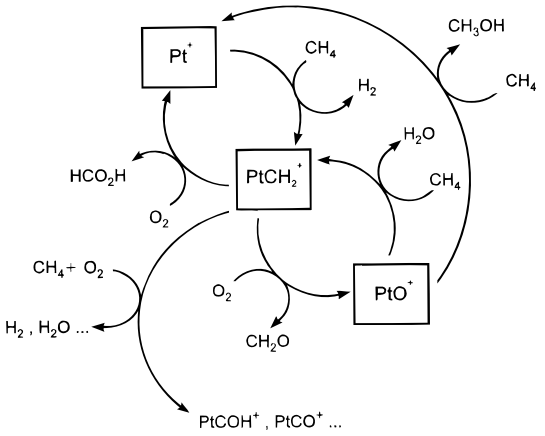

theoretical studies are indicated, although the involvement of several different spin states—e.g. doublet $Pt(CH_2)^+$, triplet O_2, and quartet Pt^+—is expected to render the calculations extremely difficult. Nevertheless, we were tempted by the task that theory could address problems that are not yet accessible by experiments and therefore started extensive calculations on the whole catalytic cycle including the elemental reactions show in Scheme 2.

An important aspect of the present calculations concerns the accuracy. For decades, calculations on transition-metal complexes were considered as extremely difficult, and only modest accuracy was achieved. In fact, comparisons between experiment and theory normally showed large errors of 10−20 kcal/mol in the computed bond strengths. However, systematic comparisons of experimental and calculated results for mainly second-row transition-metal complexes[23] revealed that the errors were highly systematic. It turned out that a simple scaling scheme (PCI-80) using a single empirical parameter was able to reproduce most of the available experimental results.[24,25] Complexes of the third transition row, where the relativistic

[⊗] Abstract published in *Advance ACS Abstracts,* February 1, 1997.

S1089-5639(96)02966-0 CCC: $14.00

SCHEME 2

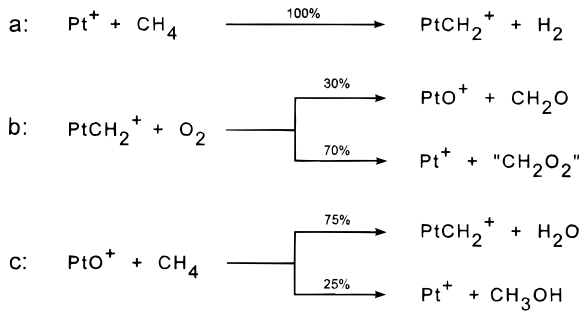

effects including spin−orbit coupling effects are large, are more challenging than those of the second row. One of the main objectives of the present study is therefore to investigate how accurate the scaling scheme is for the third row. In parallel, investigations are presently going on where the accuracy of calculations for the first transition row is studied.[26] For the first row, the presence of sometimes large near-degeneracy effects is a complicating factor. Another set of interesting computational schemes is built on density functional theory (DFT). In particular, mixed hybrid schemes including Hartree−Fock exchange, where empirical parameters are employed, have been shown to often give high accuracy for transition-metal complexes.[27−30] In the present study such a scheme (B3LYP)[31] will be used to generate results which are compared both to experiments when available and to the PCI-80 results. Furthermore, additional ion−molecule reactions were performed in an FTICR mass spectrometer to study the reverse reactions of the elementary steps in the catalytic cycle and to probe the role of possible intermediates. The experimental results are correlated with the calculated potential energy surfaces.

II. Experimental Section

All experiments were performed with a Spectrospin CMS 47X FTICR mass spectrometer equipped with an external ion source.[33,34] Pt^+ cations were generated by laser desorption/laser ionization of pure platinum[35,36] and transferred to the analyzer cell by the electromagnetic ion optics. Isolation of $^{194}Pt^+$ and all other isolation steps were performed by using FERETS.[37] The ions were thermalized by collisions with pulsed-in argon and subsequently reisolated. Experimental details of the catalytic cycle, the reactions on the $[Pt, C, H_4]^+$ hypersurface, and the generation of PtO^+ and $Pt(CH_2)^+$ have been reported previously.[17,22] $Pt(CO)^+$ and $Pt(H_2)^+$ were generated by the reaction of bare Pt^+ with pulsed-in CH_2O. Reactants were admitted to the FTICR cell at constant pressure via a leak valve. The pseudo-first-order rate constants were determined from the logarithmic decay of the precursor-ion intensity over time and are reported within ±30% error bars. The reaction efficiencies Φ were determined by dividing the experimental rate constants by the theoretical collision rates k_{ADO}.[38] The experimental results are collected in Tables 1−3.

III. Computational Details

a. Basis Sets and Methods. The calculations on the Pt^+-catalyzed oxidation of methane were performed in two steps. First, an optimization of the geometry was performed using B3LYP, a density functional theory (DFT) type of calculation based on hybrid functionals and double-ζ basis sets. In the second step the energy was evaluated for the optimized geometry using basis sets of double-ζ plus polarization quality or better. The final energy evaluation was performed both at the B3LYP level using extended basis sets and at the PCI-80 (parametrized configuration interaction with parameter 80) level.[24,25] For platinum a recently developed relativistic ECP (RECP) was used for the PCI-80 energy evaluation.[39]

TABLE 1: Experiments Relevant to the $[Pt, C, H_4]^+$ Potential Energy Surface

reaction	products	branching (ratios %)	efficiency Φ (%)
$Pt^+ + CH_4$	$Pt(CH_2)^+ + H_2$		80
$Pt^+ + CH_2D_2$	$Pt(CH_2)^+ + D_2$	10	80
	$Pt(CHD)^+ + HD$	65	
	$Pt(CD_2)^+ + H_2$	25	
$Pt(CH_2)^+ + H_2$	$Pt^+ + CH_4$		0.5
$Pt(CH_2)^+ + D_2$	$Pt(CHD)^+ + HD$	70	50
	$Pt(CD_2)^+ + H_2$	25	
	$Pt^+ + CH_2D_2$	5	

TABLE 2: Experiments Relevant to the $[Pt, C, H_2, O_2]^+$ Potential Energy Surface

reaction	products	branching ratios (%)	efficiency Φ (%)
$Pt(CH_2)^+ + O_2$	$Pt^+ + [C,H_2,O_2]$	70	4
	$PtO^+ + CH_2O$	30	
$Pt^+ + CH_2O_2$	$Pt(H_2)^+ + CO_2$	30	10
	$Pt(H_2O)^+ + CO$	50	
	$Pt(CO)^+ + H_2O$	20	
$PtO^+ + CH_2O$	$Pt^+ + [C,H_2,O_2]$	70	30
	$Pt(CO)^+ + H_2O$	30	
$Pt(CO)^+ + H_2O$	no reaction		<0.01
$Pt(H_2)^+ + CO_2$	no reaction		<0.01

TABLE 3: Experiments Relevant to the $[Pt, C, H_4, O]^+$ Potential Energy Surface

reaction	products	branching ratios (%)	efficiency Φ (%)
$PtO^+ + CH_4$	$Pt(CH_2)^+ + H_2O$	30	100
	$Pt^+ + CH_3OH$	70	
$Pt(CD_2)^+ + H_2O$	no reaction		<0.01

The geometry optimizations for most of the present systems were performed at the B3LYP level using the GAUSSIAN 94 program.[40] A few structures were optimized at the Hartree−Fock level due to convergence problems in the B3LYP calculations. Zero-point vibrational effects obtained at the Hartree−Fock level and scaled by a factor of 0.89 were added to all energies reported below.

The present DFT calculations were made using the empirically parametrized B3LYP method.[31] The B3LYP functional can be written as

$$F^{\mathrm{B3LYP}} = (1 - \mathrm{A})F_x^{\mathrm{Slater}} + AF_x^{\mathrm{HF}} + BF_x^{\mathrm{Becke}} + CF_c^{\mathrm{LYP}} + (1 - C)F_c^{\mathrm{VWN}}$$

where F_x^{Slater} is the Slater exchange, F_x^{HF} is the Hartree−Fock exchange, F_x^{Becke} is the gradient part of the exchange functional of Becke,[31] F_c^{LYP} is the correlation functional of Lee, Yang and Parr,[41] and F_c^{VWN} is the correlation functional of Vosko, Wilk, and Nusair.[42] *A*, *B*, and *C* are the coefficients determined by Becke[31] using a fit to experimental heats of formation. However, it should be noted that Becke did not use F_c^{VWN} and F_c^{LYP} in the expression above when the coefficients were determined but used the correlation functionals of Perdew and Wang instead.[32] The B3LYP method actually used was suggested by Stevens et al.[43]

The *ab initio* calculations were performed using the modified coupled pair functional (MCPF) method,[44] which is a size-consistent, single reference state method. The zeroth order wave functions were in these cases determined at the SCF level. Because rotation between valence and core orbitals sometimes

occurs a localization of the core orbitals has to be performed, and this was done using a localization procedure in which $\langle r^2 \rangle$ of the core orbitals is minimized. If standard double-ζ plus polarization (DZP) basis sets are used, it has been shown that about 80% of the correlation effects on bond strengths are obtained irrespective of the system studied. A good estimate of a bond strength is obtained by simply adding the missing 20% of the correlation effects, and this is what is done in the PCI-80 scheme.[24] The parameter 80 is thus an empirical parameter, which is not fitted but is still chosen to give agreement with experiment for a standard benchmark test[25] consisting of the 32 first-row molecules used in ref 45. For several first-row systems it was shown in ref 25 that a Hartree−Fock limit correction is also strictly needed in the PCI-80 scheme. However, this correction is usually small for transition-metal systems, and a useful procedure is to consider these effects together with basis set superposition errors and core correlation effects as included in the parametrization. This procedure has been used in the present study. The present *ab initio* calculations were performed using the STOCKHOLM set of programs.[46]

In the PCI-80 calculations the RECP[39] used for platinum treats the 4d, 5s, 5p, 5d, and 6s electrons explicitly and uses a (9*s*, 8*p*, 8*d*, 3*f*) primitive basis. The 4d core orbital is described by one contracted function, the 5*s*, 5*p*, 6*s*, and 6*p* orbitals are described by a double-ζ contraction and the 5*d* is described by a triple-ζ contraction. The *f* function was taken from Swang et al.,[47] giving a [4*s*, 4*p*, 4*d*, 1*f*] contracted basis for platinum. For carbon and oxygen the primitive (9*s*, 5*p*) basis of Huzinaga[48] was used and contracted according to the generalized contraction scheme to [3*s*, 2*p*], and one d function was added. For hydrogen the primitive (5*s*) basis from ref 48 was used, augmented with one p function and contracted to [3*s*, 1*p*].

The B3LYP energy calculations were performed using the large 6−311+G(2d,2p) basis set for hydrogen, carbon, and oxygen. This basis set has two polarization functions on all atoms. In the B3LYP calculation with this large basis set, the Hay and Wadt relativistic ECP[49] was used for platinum and the standard basis set for this ECP was expanded by uncontracting one s, one p, and one d function and by adding one diffuse d function and two f functions contracted from three primitive f functions.

In the geometry optimizations somewhat smaller basis sets were used. First, for the platinum atom the relativistic ECP according to Hay and Wadt[49] was used. The 5*s* and 5*p* core orbitals are described by a single-ζ contraction and the valence 5d, 6s and 6p orbitals by a double-ζ basis where the outermost 5d basis function is diffuse. The rest of the atoms are treated with standard double-ζ basis sets. As the single exception, the O_2 molecule was optimized with the large basis set described in the previous paragraph.

For the spin−orbit calculations described below, the inner 60 electrons of platinum ([Kr]+$4d^{10}$ +$4f^{14}$) were treated by the relativistic effective core potential given by Stevens et al.[50] The associated Gaussian-type (7s7p5d)/[4s4p3d] basis set was augmented by two f-type polarization functions (exponents: 0.2, 0.08) to generate a valence basis of triple-ζ plus two polarization functions (TZ2P) quality. For carbon and oxygen, Dunning's (11s6p)/[5s,3p] sets[51] were augmented by two d-type polarization functions (C exponents of 1.00, 0.40; O exponents of 2.56, 0.64). For hydrogen, two p-type polarization functions (exponents: 1.25, 0.45) were added to Dunning's (5s)/[3s] (311) set. All Cartesian components of the d- and f-type basis functions were retained.

b. Spin−Orbit Effects. An important aspect when calculations are performed for a heavy element like platinum is the presence of large spin−orbit effects. The energetic consequences of spin−orbit (SO) coupling on the $PtO^+ + CH_4$ potential energy surface were calculated using a semiempirical approach.[52] First, CASSCF (complete active space SCF) wave functions (active spaces described in Table 4) were computed for the electronic ground states. Their natural orbitals were used to calculate the full CI (within the CAS spaces defined in Table 4) energies of the low-lying excited states. The spin−orbit matrix elements between the ground and excited states covering a total of 5 doublet and 2 quartet states for all structures according to a calibration on $Pt(CH_2)^+$ as discussed in ref 52 were then calculated, and the spin−orbit matrix was diagonalized in order to obtain the energies of spin−orbit coupled states. Following a method elaborated by Koseki and co-workers,[53] only the one-electron part of the SO operator was used, and the missing two-electron contributions were implicitly included by introduction of "effective charges" Q_{eff}. With reference to earlier work,[52] we chose Q_{eff} (Pt) = 1200, Q_{eff} (O) = 5.6, Q_{eff} (C) 3.6, and Q_{eff} (H) = 1.0, which are optimized for the chosen basis sets and effective core potentials described in the preceding section. In the sense of valence-shell perturbation theory, the spin−orbit stabilization of a given molecular structure is defined as the energy lowering upon inclusion of SO coupling with respect to the SO uncoupled picture. The SO calculations, leading to the results in Table 4, were done using the GAMESS program system.[54] On the basis of these results, the spin−orbit effects are extrapolated for the rest of the structures in the following general way. The spin−orbit effects in Pt^+, $Pt(CH_2)^+$, and PtO^+ are assumed not to change upon complexation to closed shell molecules since no covalent bonds are formed. If the spin density on platinum is at least 0.5, a stabilization energy of 3.5 kcal/mol is added to the binding energies calculated with respect to the $5d^8\ 6s^1$ state of Pt^+ (see below). For the species where the unpaired electrons mainly are located on a ligand, a stabilization energy of 1.2 kcal/mol is used.

As mentioned above, the dissociation energies are computed using the $5d^8\ 6s^1$ asymptote of Pt^+ as reference. This procedure is used since this state is rather free of perturbations as indicated by Lande's interval rule.[55] The dissociation energy to the lowest J component of the $5d^9$ ground state is then obtained by subtracting the experimental energy difference of 27.2 kcal/mol[56] between this component and the spin−orbit averaged energy for $5d^8\ 6s^1$ and then adding the spin−orbit stabilizations in the molecules as described above.

TABLE 4: Spin−Orbit Effects on Stationary Points in the $Pt^+/CH_4/O_2$ System[a]

		CAS space[b]	E_{SO} (kcal/mol)
Pt^+ (^{2}D)		9/6	11.1[c]
$Pt(CH_2)^+$ ($^2A_1$)	MIN	15/9	3.0[c]
PtO^+ ($^4\Sigma^-$)	MIN	15/10	4.6[c]
$(H_2)Pt(CH_2)^+$ (^{2}A)	MIN	17/10	0.7
$Pt(OH)(CH_3)^+$ (^{2}A″)	TS	19/11	1.4
$Pt(OH)(CH_3)^+$ (^{2}A)	MIN	19/11	4.8
$Pt(CH_3OH)^+$ (^{2}A)	TS	19/11	3.9

[a] Minima are denoted MIN, and transition states are denoted TS. [b] no. of active electrons/no. of active orbitals. [c] From ref 52.

c. Accuracy. Many of the systems in the present study are unusually difficult to describe by quantum chemical calculations. As will be described in more detail in section IV, near degeneracy effects are often quite severe due to the presence of low lying excited states and due to breaking of bonds. Therefore, the goal of the present study is only to provide qualitatively accurate results rather than aiming for quantitative accuracy.

For many of the energies calculated in the present study, there will not be any possibility to make direct comparisons to

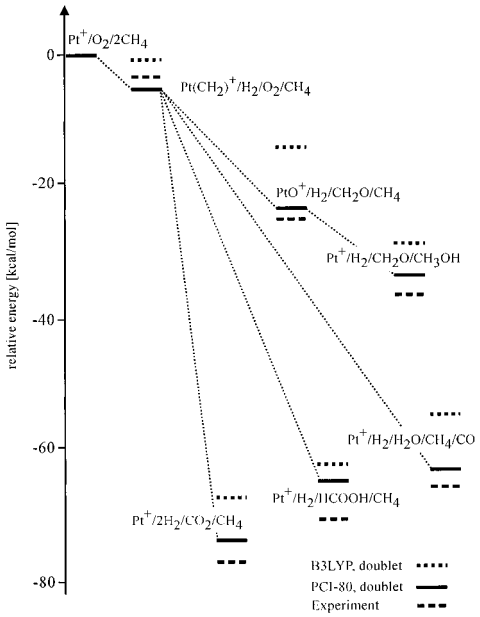

Figure 1. Energy diagram for theoretical and experimental reaction energies.

TABLE 5: Experimental and Theoretical Reaction Energies

reaction	ΔE(PCI-80) (kcal/mol)	ΔE(B3LYP) (kcal/mol)	ΔE(exptl) (kcal/mol)
$Pt^+ + CH_4 \rightarrow Pt(CH_2)^+ + H_2$	−42	−0.8	−2.9
$Pt(CH_2)^+ + O_2 \rightarrow PtO^+ + CH_2O$	−21.3	−14.1	−24.1
$Pt(CH_2)^+ + O_2 \rightarrow Pt^+ + HCOOH$	−64.2	−64.0	−71.1
$Pt(CH_2)^+ + O_2 \rightarrow Pt^+ + CO + H_2O$	−61.8	−56.7	−65.1
$Pt(CH_2)^+ + O_2 \rightarrow Pt^+ + CO_2 + H_2$	−71.0	−70.1	−75.1
$PtO^+ + CH_2O \rightarrow Pt^+ + HCOOH$	−42.9	−49.9	−47
$PtO^+ + CH_2O \rightarrow Pt^+ + CO + H_2O$	−40.5	−42.6	−41
$PtO^+ + CH_2O \rightarrow Pt^+ + CO_2 + H_2$	−49.7	−56.0	−51
$PtO^+ + CH_4 \rightarrow Pt(CH_2)^+ + H_2O$	−41.0	−44.8	−46
$PtO^+ + CH_4 \rightarrow Pt^+ + CH_3OH$	−9.8	−16.0	−11
$Pt^+ + O \rightarrow PtO^+$	−72.3	−69.3	−77
$Pt^+ + CH_2 \rightarrow Pt(CH_2)^+$	−111.9	−108.5	−112.5
$CH_4 \rightarrow CH_2 + H_2$	−107.7	−107.7	−109.6
$O_2 + 2CH_4 \rightarrow H_2 + CH_2O + CH_3OH$	−35.3	−30.8	−38.3
$O_2 + CH_4 \rightarrow 2H_2 + CO_2$	−75.2	−70.8	−78.0
$O_2 + CH_4 \rightarrow H_2 + H_2O + CO$	−66.0	−57.5	−68.0
$O_2 + CH_4 \rightarrow H_2 + HCOOH$	−68.4	−64.8	−74.4

experiment (which is of course one of the major reasons for doing the calculations), but fortunately, there are some exceptions to this. In Table 5 some results known experimentally are gathered together with comparisons to the calculated PCI-80 and B3LYP values. Comparisons between experimental and theoretical results are also illustrated in Figure 1.

The first results that can be noted in Table 5 are the binding energies of $Pt(CH_2)^+$ and PtO^+. For the low-spin $Pt(CH_2)^+$ system, the experimental value is 112.5 kcal/mol[14] and the calculated value at PCI-80 level is 111.9 kcal/mol. The corresponding B3LYP value is 108.5 kcal/mol. For the high-spin PtO^+ system, the experimental value is 77 kcal/mol[57] and the calculated PCI-80 value is 72.3. The corresponding B3LYP value is 69.3 kcal/mol.

For most of the reactions in Table 5, the calculated results are in quite good agreement with experiment. This is partly expected since the PCI-80 scheme has been shown to give an average deviation of only 2.4 kcal/mol for first-row molecules[25] and the B3LYP method, an average error of only 2.2 kcal/mol for a series of first and second-row molecules using a basis set only slightly larger than ours (6−311+G(3df,2p) as compared to ours 6−311+G(2d,2p)).[58] However, in some cases the rather small errors for the individual molecules add up and the total error becomes larger. This is the case for the reaction between O_2 and methane leading to molecular hydrogen and formic acid, where the final error is 6.0 kcal/mol using the PCI-80 scheme. The B3LYP method gives an even larger error of 9.6 kcal/mol.

TABLE 6: Relative Energies Obtained at the PCI-80 and B3LYP Levels for the Reaction $Pt^+ + CH_4 \rightarrow Pt(CH_2)^+ + H_2$[a]

molecule	structure	ΔE(PCI-80) (kcal/mol)	ΔE(B3LYP) (kcal/mol)
$Pt^+ + CH_4$		0	0
$Pt(CH_4)^+$	**1**	−25.4	−19.2
TS	**2**	−27.1	−21.2
$HPt(CH_3)^+$	**3**	−38.8	−36.7
TS	**4**	−14.2	−10.5
$HPtH(CH_2)^+$	**5**	−17.0	−15.4
TS	**6**	−10.2	−6.4
$(H_2)Pt(CH_2)^+$	**7**	−16.6	−15.6
$Pt(CH_2)^+ + H_2$		−4.2	−0.8

[a] The spin state for all structures is doublet. TS stands for transition state.

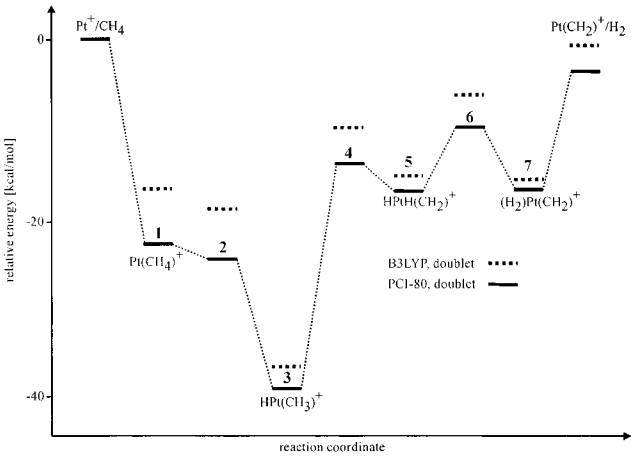

Figure 2. Potential energy curves at the PCI-80 and the B3LYP level for the reaction between Pt^+ and CH_4.

IV. Results and Discussion

a. The Reaction between Pt^+ and Methane. The first part of the Pt^+-catalyzed oxidation of methane is the reaction between Pt^+ and methane (Scheme 2, reaction a) leading to a metal carbene and molecular hydrogen. This reaction has been studied in detail recently by Heinemann et al.[17] The study in ref 17 was performed at the B3LYP level, using a somewhat smaller basis set (standard double-ζ basis with a single set of polarization functions on carbon and hydrogen and one additional diffuse d function on platinum) than the one presently used in the B3LYP energy calculations. Yet, the results obtained in the present study at the B3LYP level are rather similar to the ones in ref 17 as we will see examples of below. Zero-point corrections and spin−orbit stabilizations are added to the results in ref 17 in order to make the results comparable at the same level as the present ones.

Although seemingly simple, the reaction between Pt^+ and CH_4 goes through several steps (eqs 1−4). The relative energies for this reaction are reported in Table 6, an energy diagram of these reaction steps is given in Figure 2, and in Figure 3, the optimized geometries for the reaction are illustrated. The first step is the association reaction forming an electrostatically bound methane complex **1**

$$Pt^+ + CH_4 \rightarrow Pt(CH_4)^+ \qquad (1)$$

Structure **1** has C_s symmetry, a Pt−C distance of 2.36 Å, and one short Pt−H distance of 1.83 Å showing considerable

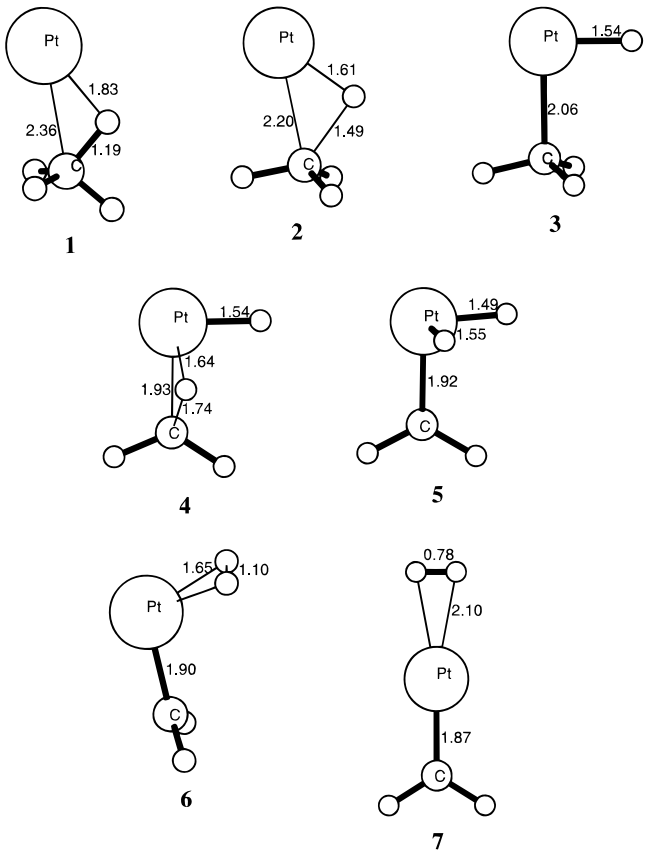

Figure 3. Structures for the intermediates in the reaction between Pt^+ and CH_4. The distances are given in angstroms.

α-agostic interaction. In this particular case, the atomic state of platinum is significantly affected by the carbon and the hydrogen atoms and the spin−orbit effects are treated in the same way as for covalently bound molecules. The B3LYP method gives a value of the binding energy to methane of 19.2 kcal/mol and the PCI-80 value is 25.4 kcal/mol. In addition to **1**, there is also another structure which has C_{2v} symmetry that is very close in energy.

The next step in the Pt^+ reaction with methane is an oxidative addition, cleaving a C−H bond and yielding the insertion product **3**, which represents the absolute minimum of the potential energy surface.

$$Pt(CH_4)^+ \rightarrow HPt(CH_3)^+ \qquad (2)$$

The relative energies in Table 6 indicate that reaction 2 is a downhill process at both the PCI-80 and the B3LYP level. The transition state **2** obtained in the geometry optimization thus disappears at a higher level of calculation. However, the change of the electronic configuration of platinum could mean that a small barrier is introduced due to a crossing of two potential surfaces corresponding to the different atomic occupations of platinum. The exothermicity for the insertion step relative to structure **1** is 13.4 kcal/mol at the PCI-80 level and 17.5 kcal/mol using B3LYP. The PCI-80 energy at this point is thus 38.8 kcal/mol below the reactants, and this is the lowest point in the reaction between Pt^+ and methane; see Figure 2. The corresponding energy obtained with B3LYP is 36.7 kcal/mol.

From the oxidative addition product **3**, the energy starts to go up. The next step is an α -hydrogen migration leading to the carbene dihydride product **5**

$$HPt(CH_3)^+ \rightarrow HPtH(CH_2)^+ \qquad (3)$$

This step has a fairly high activation energy of 24.6 kcal/mol and an endothermicity of 21.8 kcal/mol at the PCI-80 level. B3LYP gives a slightly higher activation energy of 26.2 kcal/mol and an endothermicity of 21.3 kcal/mol is obtained. The corresponding activation energy and endothermicity obtained from the results in ref 17 are 28.2 and 23.6 kcal/mol, respectively.

The origin of the rather weak binding in the dihydride carbene complex is that Pt^+ can form only three covalent bonds. Two bonds are used to bind the hydrides. The result is a single-bond character of the Pt−C bond, and the singly occupied orbital is localized on the carbon atom. The formation of more bonds would require a costly promotion to a high-lying atomic state.

The unfavorable bonding situation in complex **5** is overcome by reaction 4 which leads to structure **7**, a complex in which platinum is bound to a carbene with a double bond and to a hydrogen molecule electrostatically, leaving the unpaired electron located on the platinum atom.

$$HPtH(CH_2)^+ \rightarrow (H_2)Pt(CH_2)^+ \qquad (4)$$

The activation energy for reaching the molecular hydrogen complex **7** from the dihydride complex **5** is 6.8 kcal/mol at the PCI-80 level, and the endothermicity is 0.4 kcal/mol. This agrees well with the result obtained using B3LYP with an activation energy of 9.0 kcal/mol and an exothermicity of 0.2 kcal/mol. It also agrees rather well with the results from the studies in ref 17 where an activation energy of 9.4 kcal/mol and an exothermicity of 2.5 kcal/mol were obtained.

The final step of the methane reaction is the release of a hydrogen molecule yielding $Pt(CH_2)^+$. This step costs 12.4 kcal/mol at the PCI-80 level and 14.8 kcal/mol at the B3LYP level. The present study agrees with the result reported in ref 17 that the total process from the Pt^+ and methane reactants to the $Pt(CH_2)^+$ and H_2 product is almost thermoneutral. The value obtained here for the reaction energy using the PCI-80 scheme is 4.2 kcal/mol, compared to 0.8 kcal/mol in the B3LYP scheme. The experimental result for this process is 2.9 kcal/mol, which is based on a recently determined value of 112.5 kcal/mol for the $Pt^+-(CH_2)$ bond strength.[14] Our PCI-80 value for this bond strength is 111.9 kcal/mol. At the B3LYP level, a slightly weeker bond strength of 108.5 kcal/mol is obtained. For the process where methane is split up into methylene and molecular hydrogen, the experimental value is 109.6 kcal/mol. At both the PCI-80 and the B3LYP level the result for this reaction is 107.7 kcal/mol.

The Pt−C bond distance in $Pt(CH_2)^+$ is 1.84 Å, which is quite close to the Pt−O bond distance of 1.81 Å in PtO^+ indicating similar degrees of double-bond character. For comparison, the experimental bond distance in neutral PtO is 1.73 Å. The FTICR experiments listed in Table 1 are in good agreement with our calculated potential energy surface (Figure 2). From the observed intramolecular kinetic isotope effect in the reaction of Pt^+ with CH_2D_2 (Table 1, reaction 2), it has been concluded that the rate-determining step in the methane activation must involve the elimination of dihydrogen from a symmetric transition structure.[22] The calculated energy profile suggests that the rearrangement of the dihydrido **5** to the dihydrogen **7** complex of $Pt(CH_2)^+$ and the dissociation of **7** into $Pt(CH_2)^+$ and H_2—both involving C_2 symmetry—are the points of maximum energy en route to the reaction products. Consequently, one would expect one of these steps to be rate determining, in agreement with the measured kinetic isotope effect. If D_2 is employed in the reaction with $Pt(CH_2)^+$ (Table 1, reaction 4), one observes mainly (95%) the thermoneutral H/D exchange to form the carbene complexes $Pt(CHD)^+$ and

TABLE 7: Relative Energies Obtained at the PCI-80 and B3LYP Levels for the Reaction $Pt(CH_2)^+ + O_2 \rightarrow PtO^+ + CH_2O$[a]

molecule	structure	ΔE(PCI-80) (kcal/mol)	ΔE(B3LYP) (kcal/mol)
$Pt(CH_2)^+ + O_2$		0	0
$Pt(CH_2)(O_2)^+$ [b]	**8**	−22.2	−8.4
TS	**9**		2.6
$Pt(CH_2OO)^+$	**10**	−26.5	−12.1
TS	**11**	−14.2	−0.6
$Pt(OOCH_2)^+$	**12**	−27.7	−19.8
$Pt(OOCH_2)^+$ (q)	**13**		−31.9
$OPt(OCH_2)^+$ (q)	**14**	−74.9	−68.6
PtO^+ (q) + CH_2O		−21.3	−14.1

[a] The quartet state structures are denoted by q. The spin state for the rest of the structures is doublet. TS stands for transition state. [b] In this case the quartet and the doublet structures are equivalent as described in the text.

$Pt(CD_2)^+$, while formation of Pt^+ and CH_2D_2 amounts only to 5% of the primary products. This implies that the kinetic bottleneck in the reverse reaction concerns the reductive elimination of Pt^+ and methane from the insertion product **3**, which is located above the entrance channel $Pt(CH_2)^+$ and H_2. The observation of facile H/D exchange in $Pt(CH_2)^+$ provides yet another experimental support for the calculated potential energy surface, demonstrating that the barriers for intramolecular hydrogen shifts are energetically lower than the exit channel. In summary, the present results seem to be in reasonable agreement with available experimental results and, in most cases, with the results obtained by Heinemann et al. in ref 17. Further, a good agreement between the PCI-80 scheme and the B3LYP method is obtained.

b. The Reaction between $Pt(CH_2)^+$ and O_2. The new aspects of the present study start when $Pt(CH_2)^+$, which is produced in the sequence of steps described in the previous subsection, reacts with an oxygen molecule (Scheme 2, reaction b). As will be shown below, both product path ways stem from a vibrationally excited $OPt(OCH_2)^+$ complex **14** as the common intermediate. This may simply release the formaldehyde ligand to form PtO^+ and CH_2O or undergo further rearrangement to regenerate the Pt^+ catalyst via loss of "CH_2O_2". Thus, we will first focus on the reaction

$$Pt(CH_2)^+ + O_2 \rightarrow PtO^+ + CH_2O \qquad (5)$$

The relative energies involved in this reaction are given in Table 7, and an energy diagram for the different steps is given in Figure 4. In Figure 5, the optimized geometries for both transition states and minima are illustrated. This reaction is very difficult to describe theoretically, and therefore results of only qualitative accuracy can be expected. There are several problems involved. The most severe of these is the presence of very large near-degeneracy effects. $Pt(CH_2)^+$ is a doublet state, PtO^+ a quartet state, and the oxygen molecule a triplet state. The combined system will have ground state doublet spin for most molecular arrangements studied here. In the process of forming these doublet states and when the O−O bond is broken, large near-degeneracy effects appear. Since the spin−orbit coupling is very large for platinum, this can also lead to spin−orbit induced crossings between quartet and doublet surfaces which are difficult to locate. And indeed, it has been shown experimentally that the reaction between $Pt(CH_2)^+$ and O_2 generates platinum cations in their $^4F_{9/2}$ excited state.[17]

Finally with one or three open shells present, the occupancy of the orbitals can change very quickly from one point on the potential surface to another. One of the main reasons for these

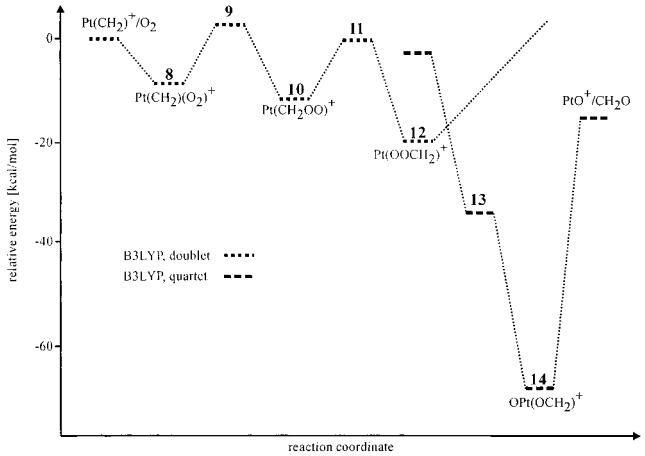

Figure 4. Potential energy curves at the B3LYP level for the reaction between $Pt(CH_2)^+$ and O_2.

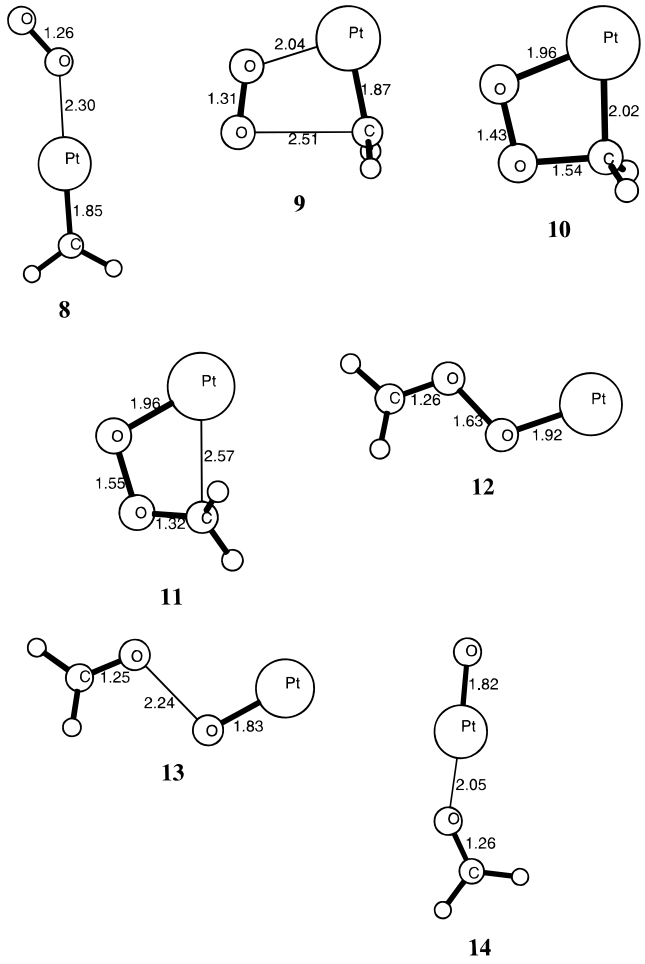

Figure 5. Structures for the intermediates in the reaction between $Pt(CH_2)^+$ and O_2. The distances are given in angstroms.

changes is that the platinum cation can use either the ground $5d^9$ state or the low-lying excited $5d^8\ 6s^1$ state to form bonds to the ligands. As can be noted in Table 7 and in the discussions below, there are often large discrepancies between the B3LYP results and the PCI-80 results for the different steps involved in reaction 5. For some structures, the PCI-80 values are even omitted. One reason for this is the rather large difference obtained for the binding energy of O_2 between the two methods. Another reason is that it is sometimes impossible to obtain convergence to the same electronic configuration in the PCI-80 and the B3LYP calculations. Futhermore, large near-degeneracy effects lead to an overestimation of the correlation

energy in the PCI-80 calculations and thus to too low energies. Because of all these circumstances, only the B3LYP results are shown in Figure 4.

The initial step of the reaction between $Pt(CH_2)^+$ and O_2 is the formation of an electrostatically bound complex **8** between the two reactant molecules. Since the total spin state of the reactants adds up to either a quartet or a doublet, and since no covalent bonds are formed, the quartet and the doublet state structure for such a complex should be equivalent. This reasoning is also confirmed from calculations at the B3LYP level in which both quartet and doublet state calculations on this complex yielded the same result. The binding energy for **8** was obtained to be 8.4 kcal/mol at the B3LYP level. At the PCI-80 level a much larger binding energy, for a quartet state calculation, of 22.2 kcal/mol was obtained.

The next step in the reaction between $Pt(CH_2)^+$ and O_2 is the one that turned out to be most problematic to describe of all the present reaction steps. In this step a four-membered ring system **10** is formed

$$Pt(CH_2)^+ + O_2 \rightarrow Pt(CH_2OO)^+ \qquad (6)$$

The $Pt(CH_2OO)+$ metallacycle **10** is a key intermediate, and its geometric features are shown in detail in Figure 5. This intermediate has to be passed in order to form PtO^+ which is itself used in the subsequent steps to complete the catalytic cycle, depicted in Scheme 1. The quantum chemical description of this doublet system is rather difficult since there are quite large near degeneracy effects. The PCI-80 reaction energy for the step when the metallacycle **10** is formed from $Pt(CH_2)^+$ and O_2 is exothermic by 26.5 kcal/mol. At the MCPF level, configurations with coefficients as large as 0.30 appear, which casts some doubt on the PCI-80 accuracy. At the B3LYP level the reaction energy for this step is only 12.1 kcal/mol. To locate the transition state for the formation of the metallacycle turned out to be extremely hard. Several different methods were tried. At the B3LYP level there is strong spin contamination of the wave function. However, a transition state **9** is found, and the energy is 2.6 kcal/mol above the entrance channel at the B3LYP level. The MCPF wave function for this structure has such large coefficients (>0.30) that the MCPF results are not reliable, and therefore, neither are the PCI-80 results. Since B3LYP also inherently is a single configurational type method, the results using this method should also be uncertain. However, the experimental results given in Table 2 strongly support the barrier obtained at the B3LYP level. The low efficiency for reaction 6 of only 4% indicates the presence of a small barrier. Although the ICR experiments are carried out under thermal conditions, a barrier of ca. 3 kcal/mol can be surmounted. For example, the reaction between $Pt(CH_2)^+$ and H_2 to form Pt^+ and CH_4 is slightly endothermic but can be observed experimentally; see Table 1. Ideally a multireference approach (MR-ACPF) should be used for this type of problem, but when this was attempted, it was only possible to include the most important configurations as reference states and the result was still not accurate. However, the most severe problem in this context is that an appropriate scaling procedure to account for the basis set limitations of the type used in PCI-80 is not yet developed for the general multireference case. Using a straightforward PCI-80 scaling of the MR-ACPF results leads to unreasonably large barriers. Since the reaction of $Pt(CH_2)^+ + O_2$, (Scheme 2, reaction b) is observed in the FTICR under thermal conditions (see Table 2), it can be concluded that the formation of the metallacycle involves only barriers of a maximum height of 3 kcal/mol. Other MCSCF-based methods like CASSCF[59] and CASPT2[60] have similar problems. In order to obtain reasonable results using these methods, it would be necessary to include the platinum d orbitals, the Pt−C bond, and the oxygen p orbitals in the active space, which is very much more than what at present is technically feasible. Even if it would be possible, the basis set problem would then be formidable on top of this. This leaves two possibilities to interpret the experimental results. The first one is that the results at the B3LYP level actually are correct, even though the multireference character of the wave function does not support this viewpoint. The formation of **10** should then proceed entirely on the doublet surface. The second possibility is that the formation of the metallacycle occurs through a spin−orbit-induced crossing between the quartet and the doublet states. The calculations indicate that the quartet state is reasonably low in energy in the region where the B3LYP method gives a transition state on the doublet surface.

The charge in the $Pt(CH_2OO)^+$ metallacycle **10** is mainly located on the platinum atom (+0.82), while the spin is mostly located on the two oxygen atoms, with the largest component on the oxygen directly binding to Pt. This electronic structure is obtained from a mixture of different valence bond configurations. One of these configurations can clearly be seen in the corresponding restricted open shell Hartree−Fock-optimized geometry. In this structure, Pt^+ in its ground state $5d^9$ configuration forms a single bond to carbon in the triplet state of CH_2O_2 leaving an unpaired electron on the oxygen atoms, mainly located on the terminal oxygen. This electronic configuration has no spin density on the platinum atom. The interaction between platinum and the terminal oxygen is mainly electrostatic in this configuration. The second valence bond configuration is one where the low-lying $5d^8\ 6s^1$ state of platinum forms two covalent bonds to the triplet state of CH_2O_2, one bond to carbon and one to the terminal oxygen. This electronic configuration leaves one unpaired electron on platinum and will therefore have the main spin density on platinum. In the B3LYP optimization this latter configuration becomes involved leading to a final spin density on platinum of 0.17 electrons and also leading to a short Pt−O distance (1.96 Å).

The first step after the formation of **10** is to break up the cycle at the Pt−C bond, leading to a $O-O-CH_2$ chain **12** bound to platinum at the terminal oxygen atom

$$Pt(CH_2OO)^+ \rightarrow Pt(OOCH_2)^+ \qquad (7)$$

The $Pt(OOCH_2)^+$ system **12** is formed in eq 7 via the transition state **11** with an activation energy of 12.3 kcal/mol and an exothermicity of 1.2 kcal/mol at the PCI-80 level. At the B3LYP level an activation energy of 11.5 kcal/mol and an exothermicity of 7.7 kcal/mol were obtained.

The charge in the transition state **11** is somewhat more delocalized than in **10**, leaving a positive charge of 0.59 on platinum and the spin mainly located on platinum (0.76) with some delocalization on the two oxygen atoms. The electronic configuration in this structure is a mixture between the one in the metallacycle **10** involving the d^9 state on platinum and the one on the chain structure **12** to be described below. Compared to the metallacycle **10**, the Pt−C bond length in the transition state structure **11** is significantly increased, since this is the bond to be broken. Furthermore, the C−O and the O−O bonds are changed accordingly to become closer to the singlet state of CH_2O_2, which is dominating in the chain structure. This transition state **11** can thus be described as a transition from the triplet state of CH_2O_2 binding covalently to platinum via the carbon to the singlet state of CH_2O_2 binding electrostatically to platinum via the oxygen atom.

Most of the charge in the $Pt(OOCH_2)^+$ chain structure **12** is located on platinum (+0.83), and the spin is completely located

on platinum (1.0). The electronic structure of this molecule mainly corresponds to the ground d^9 state of platinum, electrostatically interacting with the singlet state of CH_2O_2.

The reaction is completed by the cleavage of the O−O bond to form formaldehyde, either in free form to yield PtO^+ or electrostatically bound in a $OPt(OCH_2)^+$ complex that undergoes additional reactions (see below)

$$Pt(OOCH_2)^+ \rightarrow PtO^+ + CH_2O \qquad (8)$$

No transition state was located for this step. The dissociation reaction for liberating formaldehyde from **12** appears to proceed through an initial spin−orbit-induced crossing over to a quartet state of the linear chain. The crossing region was roughly estimated by performing a geometry optimization for the quartet state by keeping the same bond distance between the oxygen atoms as in the doublet chain structure **12** and optimizing the rest of the geometry parameters. The energy for this structure on the quartet surface was obtained to be higher in energy than **12** by 23.8 kcal/mol at the PCI-80 level and by 18.6 kcal/mol at the B3LYP level. Starting from this structure and performing a full optimization for the quartet state leads to the structure **13** which is found to be bound by 31.9 kcal/mol relative to $Pt(CH_2)^+ + O_2$ at the B3LYP level. This implies that there is no barrier on the quartet surface for breaking the O−O bond and that the crossing between the doublet and quartet surfaces should occur well below the $Pt(CH_2)^+ + O_2$ asymptote.

The quartet structure **13** mentioned above is shown in Figure 5. Here it can be seen that the O−O bond is broken and the formaldehyde molecule is thus only electrostatically interacting with PtO^+. This structure is at most a local minimum which, via a small barrier, can transform into the very strongly bound electrostatic complex **14**. This complex contains a formaldehyde ligand which is coordinated directly to platinum and bound by 68.6 kcal/mol relative to $Pt(CH_2)^+ + O_2$ at the B3LYP level and by 74.9 kcal/mol at the PCI-80 level. Finally, the quartet PtO^+ and free formaldehyde dissociate without any additional barrier in an uphill reaction.

c. The Further Reaction of $OPt(OCH_2)^+$. In the actual catalytic cycle, formation of PtO^+ and CH_2O from $Pt(CH_2)^+$ and O_2 (Scheme 2, reaction b) corresponds to only 30% of the reaction products. Thus, we conclude that the major part of **14** undergoes further rearrangement to finally yield Pt^+ and neutral "CH_2O_2" instead of simply detaching the formaldehyde ligand. While already the calculations suggest that **14** is an intermediate en route to regenerate the platinum catalyst, this assumption is supported by the ion−molecule reaction of thermalized PtO^+ with CH_2O (Table 2), which also generates mostly Pt^+ and "CH_2O_2". Besides these products also water and Pt(CO)+ are obtained. The latter products are not observed in the catalytic cycle, and this difference can be rationalized by the higher entrance energy of $Pt(CH_2)^+/O_2$ compared to PtO^+/CH_2O. Since the identity of the neutrals CH_2O_2 formed in reaction b can not be determined in the ICR experiments, three different path ways have to be considered. The first one leads to formation of formic acid

$$OPt(OCH_2)^+ \rightarrow Pt^+ + HCOOH \qquad (9)$$

The second one leads to formation of carbon monoxide and water

$$OPt(OCH_2)^+ \rightarrow Pt^+ + CO + H_2O \qquad (10)$$

And the third one leads to formation of carbon dioxide and a hydrogen molecule

$$OPt(OCH_2)^+ \rightarrow Pt^+ + CO_2 + H_2 \qquad (11)$$

The relative energies for the detailed reaction steps in eqs 9−11 are reported in Table 8. In Figure 6, energy diagrams for these reactions are shown, and the geometries for the structures involved in the reactions 9−11 are illustrated in Figure 7. Since PtO^+ has a quartet ground state, so has the electrostatic complex $OPt(OCH_2)^+$ **14**, which is bound by 54.5 kcal/mol relative to PtO^+ and CH_2O at the B3LYP level. At the PCI-80 level a very similar result of 53.6 kcal/mol was obtained, even though a coefficient of 0.30 appeared in the MCPF expansion. The bond strength on the doublet potential surface is found to be 44.6 kcal/mol at the PCI-80 level. In the B3LYP calculation, which is of unrestricted type, the doublet states of PtO^+ and $OPt(OCH_2)^+$ are partly spin contaminated by the quartet ground states and the B3LYP energies are therefore not reliable, and only PCI-80 energies are available for these systems. As will be seen in the next paragraph, there is only a very low barrier on the doublet surface after the $OPt(OCH_2)^+$ molecular complex is formed, and it is therefore questionable if such a complex really exists. However, the low energy obtained in this region on the doublet surface indicates that the spin crossing, which precedes the formation of the C−H insertion product, occurs at a low energy and does not involve a barrier located above the entrance channel energy.

The next step in the formaldehyde reaction sequence is an oxidative addition breaking the formaldehyde C−H bond

$$OPt(OCH_2)^+ \rightarrow OPtH(CHO)^+ \qquad (12)$$

On the doublet surface, a transition state **15**, shown in Figure 7, is located for this step yielding a very low barrier of 1.7 kcal/mol at the PCI-80 level without zero-point vibration energy. When the zero-point vibration energy is added, **15** becomes 3.0 kcal/mol more bound than the doublet state of $OPt(OCH_2)^+$, and the barrier on the doublet surface thus disappears. However, relative to the quartet state of $OPt(OCH_2)^+$, **14**, the transition state **15** is still unbound by 34.7 kcal/mol at the PCI-80 level and by 40.1 kcal/mol at the B3LYP level. As mentioned above, a barrier has to occur due to the spin crossing between the doublet and quartet surface in this region. Reaction 12 has an exothermicity of 24.3 kcal/mol at the PCI-80 level. The most notable feature of the transition state **15** is the long Pt−C bond distance of 3.02 Å. After it is passed, the platinum−carbon bond is considerably shortened resulting in a Pt−C bond length of 2.08 Å in the inserted product **16**. The Pt−O distance is 1.88 Å and thus not drastically elongated as compared to **14**.

The next step, also in common for all the reactions 9−11, brings about formation of a hydroxyl ligand resulting in structure **18**

$$OPtH(CHO)^+ \rightarrow Pt(OH)(CHO)^+ \qquad (13)$$

The exothermicity of this step is 42.1 kcal/mol at the PCI-80 level and 43.2 kcal/mol at the B3LYP level. The product **18** is reached after passing a barrier (structure **17**) of 7.9 kcal/mol at the PCI-80 level, while the B3LYP calculation gives a somewhat larger barrier of 12.8 kcal/mol.

Intermediate **18** has two options to react further. The first one is reductive elimination of formic acid

$$Pt(OH)(CHO)^+ \rightarrow Pt(HCOOH)^+ \qquad (14)$$

This process is endothermic by 5.2 kcal/mol at the PCI-80 level and exothermic by 0.6 kcal/mol at the B3LYP level. The reaction goes over a barrier **19** of 22.5 kcal/mol at the PCI-80

TABLE 8: Relative Energies Obtained at the PCI-80 Level and at the B3LYP Level for the Further Reactions of $OPt(OCH_2)^+$ [a]

molecule	structure	ΔE(PCI-80) (kcal/mol)	ΔE(B3LYP) (kcal/mol)
$Pt(CH_2)^+ + O_2$		0	0
$OPt(OCH_2)^+$ (q)	**14**	−74.9	−68.6
$OPt(OCH_2)$		−37.2	
TS	**15**	−40.2	−28.5
$OPtH(CHO)^+$	**16**	−61.5	−53.9
TS	**17**	−53.6	−41.1
$Pt(OH)(CHO)^+$	**18**	−103.6	−97.1
TS	**19**	−81.1	−68.8
$Pt(HCOOH)^+$	**20**	−98.4	−97.7
$Pt^+ + (HCOOH)$		−64.2	−64.0
TS	**21**	−85.6	−68.8
$HPt(OH)(CO)^+$	**22**	−128.0	−123.0
TS	**23**	−111.0	103.5
$(H_2O)Pt(CO)^+$	**24**	−170.5	−158.8
$Pt(CO)^+ + H_2O$		−121.5	−113.0
$Pt^+ + CO + H_2O$		−61.8	−56.7
TS	**25**	−57.4	−47.3
$H_2PtO(CO)^+$	**26**	−60.6	−48.4
TS	**27**	−62.4	−36.9
$H_2Pt(CO_2)^+$	**28**	−128.0	−126.5
$Pt(H_2)^+ + CO_2$		−103.3	−95.5
$Pt^+ + CO_2 + H_2$		−71.0	−70.1

[a] The quartet state structures are denoted by q. The spin state for the rest of the structures is doublet. TS stands for transition state.

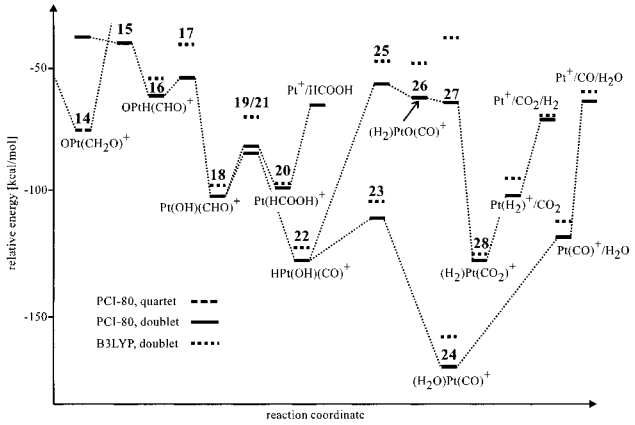

Figure 6. Potential energy curves at the PCI-80 and the B3LYP level for the reactions between PtO^+ and CH_2O.

level and 28.3 kcal/mol at the B3LYP level. Formic acid can be released at the cost of the electrostatic binding energy which amounts to 34.2 kcal/mol at the PCI-80 level and 33.7 kcal/mol at the B3LYP level. The overall exothermicity for the formation of formic acid from $Pt(CH_2)^+ + O_2$ is then 64.2 kcal/mol at the PCI-80 level and 64.0 kcal/mol at the B3LYP level. The experimental value is 71.1 kcal/mol.

The second path way commencing from the intermediate **18** formed in eq 13, is an α -elimination type step (i.e. the reversal of a carbonyl insertion) leading to the cleavage of the C−H bond in the formyl group

$$Pt(OH)(CHO)^+ \rightarrow HPt(OH)(CO)^+ \qquad (15)$$

This step goes over a barrier of 18.0 kcal/mol at the PCI-80 level and 28.3 kcal/mol at the B3LYP level. It is exothermic by 24.4 kcal/mol at the PCI-80 level and by 25.9 kcal/mol at the B3LYP level. The PCI-80 value for the transition state is doubtful since a large coefficient appeared in the MCPF calculation. The product $HPt(OH)(CO)^+$ complex **22** has C_s symmetry ($^2B'$), and the unpaired electron is located mostly on the oxygen binding to platinum.

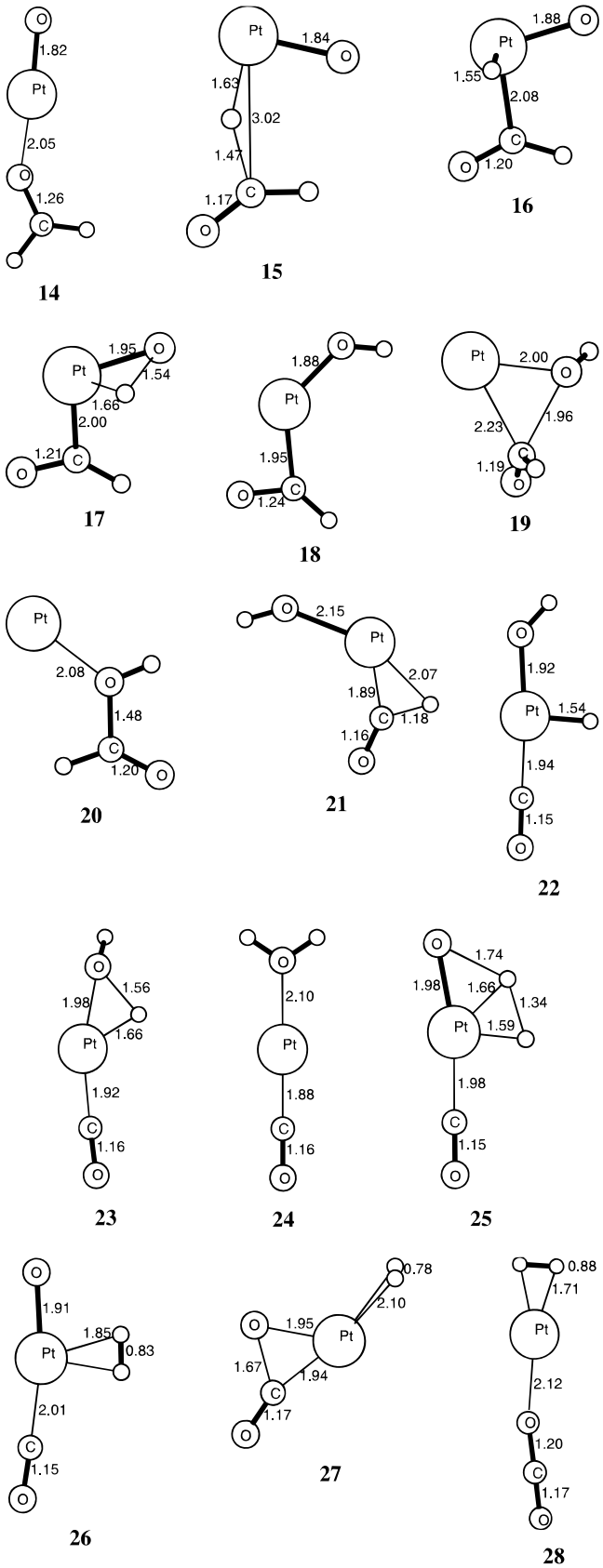

Figure 7. Structures for the intermediates in the reactions between PtO^+ and CH_2O. The distances are given in angstroms.

The product **22** formed in eq 15 can undergo reductive elimination via the transition state structure **23** to form an electrostatically bound water ligand in complex **24**

$$HPt(OH)(CO)^+ \rightarrow (H_2O)Pt(CO)^+ \qquad (16)$$

At the PCI-80 level, this step has a barrier of 17.0 kcal/mol and is exothermic by 42.5 kcal/mol. The corresponding B3LYP values are 19.5 and 35.8 kcal/mol, respectively. To release both carbon monoxide and water from **24** costs 102.1 kcal/mol at the B3LYP level. At the PCI-80 level an even larger binding energy of 108.7 kcal/mol was obtained. With all these steps added, the overall reaction exothermicity for forming carbon monoxide and water from $Pt(CH_2)^+$ and molecular oxygen becomes 61.8 kcal/mol using the PCI-80 scheme and 56.7 kcal/mol at the B3LYP level, which can be compared to the experimental value of 65.1 kcal/mol.

To complete the overall reaction 11 two steps are needed from the complex **22**. The first step is the dissociation of the O-H bond of the hydroxyl group in **22** leading to the formation of a complex with an electrostatically bound hydrogen molecule **26**

$$HPt(OH)(CO)^+ \rightarrow (H_2)PtO(CO)^+ \qquad (17)$$

This process has an activation energy of 70.6 kcal/mol at the PCI-80 level and an endothermicity of 67.4 kcal/mol. The corresponding B3LYP results are 75.7 and 74.6. Thus, both methods show that the energy difference between the transition state **25** and the product **26** is very small and the reaction proceeds with almost no extra barrier on top of the endothermicity. The spin in **26** is located mostly on the oxygen closest to platinum, and the complex has C_s symmetry ($^2A'$).

The final step of the overall reaction 11 is a reductive elimination of carbon dioxide yielding complex **28**

$$(H_2)PtO(CO)^+ \rightarrow (H_2)Pt^+(CO_2) \qquad (18)$$

This step is found to have an exothermicity of 67.4 kcal/mol at the PCI-80 level and 78.1 kcal/mol at the B3LYP level. At the B3LYP level an activation energy of 11.5 kcal/mol was obtained. At the PCI-80 level the transition state **27** optimized at the B3LYP level is no longer a true transition state. However, this PCI-80 result is somewhat unreliable, since an expansion coefficient as large as 0.26 occurs in the MCPF wave function.

The release of the electrostatically bound carbon dioxide and a hydrogen molecule from **28** costs 57.0 kcal/mol at the PCI-80 level and 56.4 kcal/mol at the B3LYP level. The PCI-80 result for the total reaction exothermicity for forming carbon dioxide and molecular hydrogen from $Pt(CH_2)^+ + O_2$ is thus 71.0 kcal/mol, and the corresponding B3LYP result is 70.1 kcal/mol, both in fair agreement with the experimental value of 75.1 kcal/mol. In summary, the calculations show that all three different path ways proceed well below the entrance channel of $Pt(CH_2)^+$ and O_2. Thus, it is most likely that a mixture of the different products HCOOH, H_2O/CO, and H_2/CO_2 is formed in the catalytic cycle. This is also suggested by the reaction of $Pt^+ + HCOOH$ where CO_2, CO, or H_2O are released as neutral products (see Table 2) which implies that, even if formic acid is formed in the oxidation, it could be decomposed on the metal center. The reaction of bare Pt^+ with formic acid provides yet some support for the calculated potential energy surface; the entrance energy of this reaction lies well above all stationary points to proceed to $Pt(CO)^+/H_2O$ and $Pt(H_2O)^+$/CO, and both products are observed experimentally. In addition, the calculations show that formation of $Pt(H_2)^+$ and CO_2 from Pt^+ and formic acid is an exothermic process and involves only, if any at all, a slight barrier. In fact, these products are also found experimentally, and although they might be formed via an alternative pathway, e.g. initial activation of the C−H bond, this result still supports the calculated thermochemistry. Furthermore, according to the calculations, the reaction of $Pt(H_2)^+$ and CO_2 to $Pt(CO)^+$ and H_2O would be exothermic by about 17 kcal/mol, but kinetic barriers for the structures **25**−**27** lie well above the entrance energy. So it is not surprising that this reaction does not occur in the ICR experiment. The same line of arguments also explains why experimentally $Pt(CO)^+$ proves to be unreactive toward H_2O.

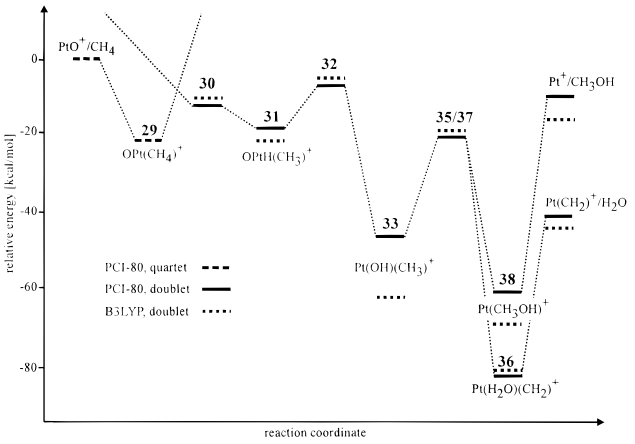

Figure 8. Potential energy curves at the PCI-80 and the B3LYP level for the reactions between PtO^+ and CH_4.

d. The Reaction between PtO^+ and CH_4. As discussed above, PtO^+, which is yielded in reaction 5, also takes part in the catalytic process since it efficiently reacts with methane (see Scheme 2).

There are two different product channels in the reaction with methane, and the first one results in a generation of $Pt(CH_2)^+$

$$PtO^+ + CH_4 \rightarrow Pt(CH_2)^+ + H_2O \qquad (19)$$

$Pt(CH_2)^+$ can then be used to restart the reaction with O_2 as described in subsection b. The second reaction sequence results in formation of methanol which is one of the important products in this catalytic process.[3] The overall reaction in this case is

$$PtO^+ + CH_4 \rightarrow Pt^+ + CH_3OH \qquad (20)$$

In the experiment a 30% yield of methanol is obtained in the reaction between PtO^+ and methane. The remaining 70% are due to reaction 19. The energy diagram for the different steps of the reaction between PtO^+ and methane is given in Figure 8.

The initial step in the reaction between PtO^+ and methane is the formation of an electrostatically bound complex in **29**

$$PtO^+ + CH_4 \rightarrow OPt(CH_4)^+ \qquad (21)$$

Since PtO^+ has a quartet ground state with an excitation energy to the doublet state of 28.7 kcal/mol at the PCI-80 level, also the methane complex **29** has a quartet ground state. The bond strength to methane is 27.1 kcal/mol for the quartet state of PtO^+ at the PCI-80 level, which is significantly less than the corresponding binding energy of formaldehyde to PtO^+ in the complex **14** of 53.6 kcal/mol. The main difference between these two complexes is that formaldehyde coordinates with an oxygen lone pair to the platinum atom, while methane coordinates with C−H bonds, which thus only give about half of the oxygen lone-pair coordination energy. Another comparison that can be of interest is between Pt^+ and PtO^+ coordination of methane. In the $Pt(CH_4)^+$ complex **1**, methane is bound by 25.4 kcal/mol at the PCI-80 level, which is thus only slightly less than in the complex **29**. As mentioned above, the B3LYP wave function for the doublet of PtO^+ is spin contaminated by

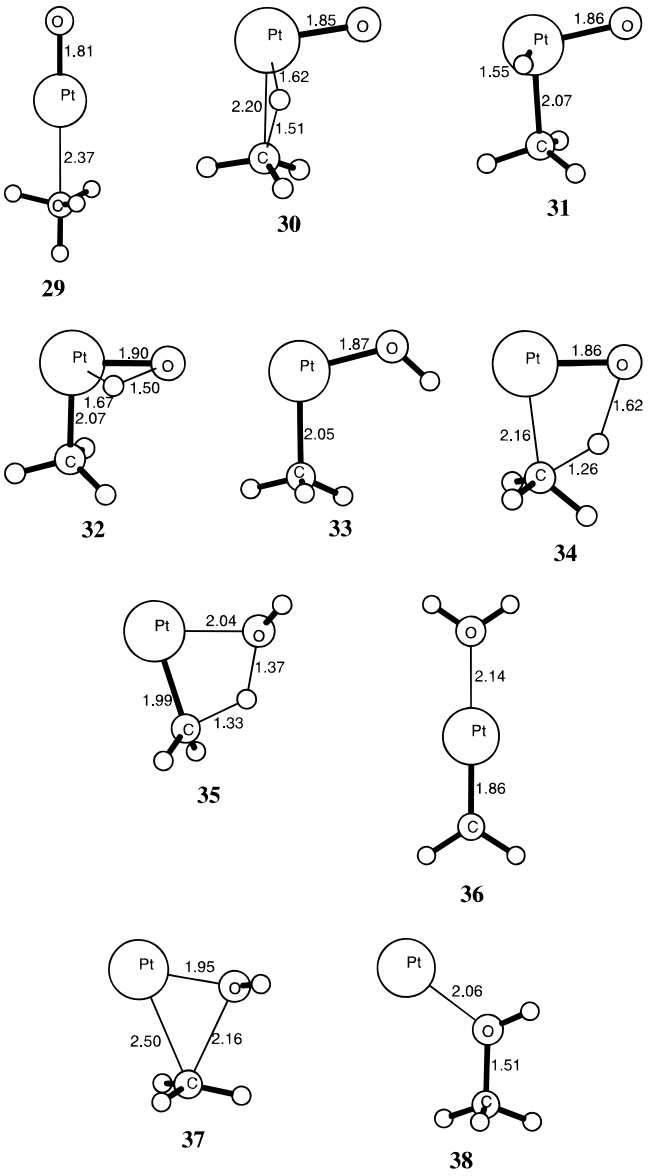

Figure 9. Structures for the intermediates in the reactions between PtO^+ and CH_4. The distances are given in angstroms.

the ground state quartet, and therefore no reliable results for bonding in the doublet state of $OPt(CH_4)^+$ could be obtained.

In the second step of this sequence, the electrostatically bound methane in **29** undergoes oxidative addition breaking a C−H bond leading to product **31**

$$OPt(CH_4)^+ \rightarrow OPtH(CH_3)^+ \qquad (22)$$

This reaction can easily occur only on the doublet surface where it is downhill at the PCI-80 level. The transition state **30** obtained at the B3LYP level is thus not a true transition state at the PCI-80 level. Since the C−H bond breaking has a very high barrier for the quartet state, there will be a curve crossing between the quartet and the doublet states in this region. The subsequent steps of this reaction then occur on the doublet surface. The result that the C−H bond insertion only proceeds on the low-spin surface and is hindered by a high barrier on the high-spin surface is generally found for most transition-metal complexes.[4] The reason for this is that a low spin is needed for an easy recoupling of the bonding electrons. The doublet product of the oxidative addition, complex **31**, and the transition-state structure obtained in the B3LYP optimization both have, in their ground states, the spin mainly located on oxygen, which means that the spin−orbit effects in these structures are almost quenched. The reaction mechanism is similar to the reaction step from $OPtO(CH_2)^+$ in eq 12, but it should be noted that the Pt−C bond distance for the transition states in the two reactions is very different, 3.02 Å for **15** and 2.20 Å or **30**. It was also pointed out above that the electrostatic complex formed between PtO^+ and the ligand is also entirely different in the two cases. Methane is coordinating via the C−H bonds, and formaldehyde coordinates via the oxygen lone-pairs. The formation of the $OPtH(CH_3)^+$ complex **31** from the doublet state of PtO^+ is an exothermic process with an energy gain of 48.2 kcal/mol at the PCI-80 level.

TABLE 9: Relative Energies Obtained at the PCI-80 and B3LYP Levels for the Reactions between PtO^+ and CH_4[a]

molecule	structure	ΔE(PCI-80)	ΔE(B3LYP)
PtO^+ (q) + CH_4		0	0
$OPt(CH_4)^+$ (q)	**29**	−27.1	−21.6
$PtO^+ + CH_4$		28.7	
$OPt(CH_4)^+$		20.7	
TS	**30**	−12.4	−9.7
$OPtH(CH_3)^+$	**31**	−19.5	−22.3
TS	**32**	−7.0	−5.9
$PtOH(CH_3)^+$	**33**	−46.4	−60.9
TS	**34**	−4.6	−0.9
$PtOH(CH_3)^+$	**33**	−46.4	−60.9
TS	**35**	−20.9	−16.1
$Pt(H_2O)(CH_2)^+$	**36**	−82.1	−81.1
$Pt(CH_2)^+ + H_2O$		−41.0	−44.8
TS	**37**	−20.4	−20.9
$Pt(CH_3OH)^+$	**38**	−63.7	−70.5
$Pt^+ + CH_3OH$		−9.8	−16.0

[a] The quartet state structures are denoted by q. The spin state for the rest of the structures is doublet. TS stands for transition state.

In the next step the hydride ligand on platinum migrates to the oxygen forming a hydroxyl ligand in the product complex **33**

$$OPtH(CH_3)^+ \rightarrow Pt(OH)(CH_3)^+ \qquad (23)$$

The exothermicity for this reaction step is 38.6 kcal/mol, and the activation energy is 16.4 at the B3LYP level. For the transition state **32**, the spin is mainly located on oxygen, whereas in the product **33**, the spin is equally shared between oxygen and platinum. The increase of spin density on platinum implies that larger spin−orbit effects have to be taken into account. The calculated stabilization from the spin orbit coupling in the product amounts to 4.8 kcal/mol (Table 4). At the PCI-80 level, an activation energy of 12.5 kcal/mol was obtained. For the product at the PCI-80 level, it was not possible to obtain the same occupation as was obtained in the B3LYP calculations. The PCI-80 energy for this structure **33**, given in Table 9, corresponds to a wave function in which the spin is entirely localized on platinum. The different localizations of the unpaired electron in the two methods resulted in a large difference between the reaction energies with a value of 38.6 kcal/mol at the B3LYP level and of only 26.9 kcal/mol at the PCI-80 level.

There is also another low-lying, more direct, reaction path leading to the $Pt(OH)(CH_3)^+$ product **33** from the $OPt(CH_4)^+$ **29** electrostatic complex

$$OPt(CH_4)^+ \rightarrow Pt(OH)(CH_3)^+ \qquad (24)$$

In this reaction path a metallacycle **34** serves as the transition state. The localization of the unpaired electron in the metallacycle is mainly on oxygen. The spin−orbit effects are therefore almost quenched, and the calculated stabilization for

the transition state amounts only to 1.4 kcal/mol. The energies relative to the initial reactants $PtO^+ + CH_4$ for the transition state are −4.6 kcal/mol at the PCI-80 level and −0.9 kcal/mol at the B3LYP level, which is thus very close to the zero. Both methods indicate that the reaction path in which the metallacycle transition state **34** is formed is unfavorable in comparison to the path 22−23 discussed above. The high efficiency which was found experimentally for the reaction $PtO^+ + CH_4$ also suggests that the barriers involved in the reaction pathway are well below the entrance energy.

From the $Pt(OH)(CH_3)^+$ complex **33** there are two possible paths. In the first one a hydrogen on the methyl group migrates via the transition state **35** over to the oxygen forming a water molecule.

$$Pt(OH)(CH_3)^+ \rightarrow Pt(H_2O)(CH_2)^+ \qquad (25)$$

The product complex **36** is planar and can be described as a metal−carbene complex electrostatically binding to a water molecule. The activation energy and the exothermicity for reaction 25 is 44.8 kcal/mol and 20.2 kcal/mol, respectively, at the B3LYP level. The release of water, which is endothermic by 41.1 (PCI-80) or 36.3 kcal/mol (B3LYP), respectively, completes the reaction sequence. The difference between the PCI-80 and the B3LYP results are due to the differences in the wave function for **33** discussed above. The relative energies of the exit channel and the transition state **35** are supported by another ICR experiment: in the reaction of the deuterated carbene complex $Pt(CD_2)^+$ with H_2O the thermoneutral H/D exchange could be expected, provided the absence of kinetic barriers. In fact, the barrier for insertion into the O−H bond of water **35** is calculated to be about 20 kcal/mol endothermic with respect to the reactants $Pt(CD_2)^+$ and H_2O, thus explaining why no reaction is observed experimentally. The total reaction energy of eq 19 is at the PCI-80 level 41.0 kcal/mol and at the B3LYP level 44.8 kcal/mol, compared to the experimental value of 46 kcal/mol.

In the second reaction path from **33**, a reductive elimination occurs leading to **38** where a methanol molecule is electrostatically bound to Pt^+

$$Pt(OH)(CH_3)^+ \rightarrow Pt(CH_3OH)^+ \qquad (26)$$

At the B3LYP level, the activation energy for this reductive elimination is 40.0 kcal/mol and the reaction proceeds via the transition state structure **37**. The release of methanol requires 53.9 kcal/mol at the PCI-80 level and 54.5 kcal/mol at the B3LYP level. The overall reaction energy for eq 20 is at the B3LYP level 16.0 kcal/mol and at the PCI-80 level 9.8 kcal/mol. The experimental reaction energy is 11 kcal/mol.

V. Conclusions

The different reactions involved in the Pt^+ -catalyzed oxidation of methane have been studied in detail by extensive calculations and ICR-experiments which lead to an almost complete understanding of the different elementary steps involved. Most of these steps correspond to well-known mechanisms, e.g. oxidative addition, reductive elimination, or hydrogen migration, but some less common types of reactions are also involved. The most notable example concerns the key step in the overall catalytic cycle, i.e. the reaction between $Pt(CH_2)^+$ and molecular oxygen. It proceeds through a four-membered metallacycle which is formed by [2+2] addition of O_2 to $Pt(CH_2)+$. Besides the intermediates, the products of this oxidation reaction could be established by the calculations. Most probably, the reaction is not selective and yields a mixture of formic acid and its decomposition products CO/H_2O and CO_2/H_2, respectively. Another interesting feature of the reaction sequences studied is the crossings between potential energy surfaces of different spin. It has been shown experimentally for the reaction $Pt(CH_2)^+ + O_2$ [5] that Pt^+ is partially produced in its low-lying first excited state ($^4F_{9/2}$). This is reasonable since the experimental excitation energy only amounts to 17.5 kcal/mol[56] if the weighted avarage over all spin−orbit components are used. The large spin−orbit coupling constant of the third transition-row member like platinum is here of large importance for the catalytic efficiency.

Obviously, many of the reaction steps found in the present catalytic cycle must be considered to be particular for gas-phase cationic reactions and will not occur for real homogeneous catalysts in solution. One drastic example is the formation of carbon dioxide in the reaction between $Pt(CH_2)^+$ and molecular oxygen, where one reaction step in this sequence goes over a barrier of about 70 kcal/mol, which is much too high to be observed in a solution system. To be observable at a reasonable time scale in solution, barriers cannot exceed 20−25 kcal/mol. Apart from this dynamical difference between gas phase and solution, the potential energy surfaces calculated should be reasonably representative of the energetics involved also in a solution experiment, at least if a nonpolar solvent is used. For a polar solvent like water, long range polarization can substantially modify the reaction energetics. Another difference between the present reactions and most catalytic reactions in solution is that the present study concerns cations. However, in some of the most interesting recently developed homogeneous catalysts for polymerization, for example, cationic complexes are actually the active catalysts.[61]

One of the most important reasons to perform the present set of calculations was to investigate the accuracy of the computational methods for treatment of reactions involving third-row transition metals. The conclusion from these calculations is that both the PCI-80 scheme and the B3LYP method are quite successful in reproducing the experimental results in most cases. A requirement for the high accuracy is that spin−orbit effects have been accounted for in a reasonable way. In the present reactions spin−orbit effects modify the energetics by typically 6−10 kcal/mol. However, in a few cases the computational efforts have been problematic. These cases occur where near degeneracy effects are very large involving many closely lying electronic states. In these cases both PCI-80 and B3LYP show tendencies of breakdown. Alternative multireference methods capable of handling these situations do not exist at present either, and these cases thus represent a challenge for future method development.

Acknowledgment. The work at the Technischen Universität Berlin has been funded by the Deutsche Forschungsgemeinschaft, the Volkswagen-Stiftung, and the Fonds der Chemischen Industrie. The work at Stockholm has been funded by NFR.

References and Notes

(1) Schwarz, H. *Angew. Chem., Int. Ed. Engl.* **1991**, *30*, 820.
(2) Fox, J. M. *Catal. Rev.-Sci. Eng.* **1993**, *35*, 169.
(3) Catalytic conversion of CH_4 to CH_3OH has been listed as one of the ten challenges for catalysis: *Chem. Eng. News* **1993**, *71* (May 31), 27.
(4) Crabtree, R. H. *Chem. Rev.* **1995**, *95*, 987.
(5) Olah, G.; Molnar, A. *Hydrocarbon Chemistry:* Wiley: New York, 1995.
(6) van Koppen, P. A. M.; Kemper, P. R.; Bushnell, J. E.; Bowers, M. T. *J. Am. Chem. Soc.* **1995**, *117*, 2098.
(7) Schröder, D.; Schwarz, H. *Angew. Chem. Int. Ed. Engl.* **1990**, *29*, 1433.
(8) Tjelta, B. L.; Armentrout, P. B. Submitted to *J. Am. Chem. Soc.*

(9) Irikura, K. K.; Beauchamp, J. L. *J. Am. Chem. Soc.* **1989**, *111*, 75.
(10) Irikura, K. K.; Beauchamp, J. L. *J. Am. Chem. Soc.* **1991**, *113*, 2769.
(11) Irikura, K. K.; Beauchamp, J. L. *J. Phys. Chem.* **1991**, *95*, 8344.
(12) Lias, S. G; Liebman, J. F; Levin, R. D.; Kafafi, S. A. *NIST Standard Reference Database, Positive Ion Energetics, Version 2.01*, Gaithersburg, MD, January, 1994.
(13) Heinemann, C.; Hertwig, R. H.; Wesendrup, R.; Koch, W.; Schwarz, H. *J. Am. Chem. Soc.* **1995**, *117*, 495.
(14) Heinemann, C.; Schwarz, H.; Koch, W.; Dyall, K. G. *J. Chem. Phys.* **1996**, *104*, 4642.
(15) Perry, J. K.; Ohanessian, G.; Goddard, W. A. *Organometallics* **1994**, *13*, 1870.
(16) Musaev, D. G.; Morokuma, K. *Isr. J. Chem.* **1993**, *33*, 307.
(17) Heinemann, C.; Wesendrup, R.; Schwarz, H. *Chem. Phys. Lett.* **1995**, *239*, 75.
(18) (a) Co^+: Musaev, D. G.; Morokuma, K.; Koga, N.; Nguyen, K. A.; Gordon, M. S.; Cundari, T. R. *J. Phys. Chem.* **1993**, *97*, 11435. (b) Hendrickx, M.; Ceulemans, M.; Vanquickenborne, L. *Chem. Phys. Lett.* **1996**, *257*, 8.
(19) Rh^+: Musaev, D. G.; Koga, N.; Morokuma, K. *J. Phys. Chem.* **1993**, *97*, 4064.
(20) Y^+-Pd^+ : Blomberg, M. R. A.; Siegbahn, P. E. M.; Svensson, M. *J. Phys. Chem.* **1994**, *98*, 2062.
(21) Musaev, D. G.; Morokuma, K. *J. Phys. Chem.* **1996**, *100*, 11600.
(22) Wesendrup, R.; Schröder, D.; Schwarz H., *Angew. Chem., Int. Ed. Engl.* **1994**, *33*, 1174.
(23) Carroll, J. J.; Weisshaar, J. C.; Blomberg, M. R. A.; Siegbahn, P. E. M.; Svensson, M. *J. Phys. Chem.* **1995**, *99*, 13955.
(24) Siegbahn, P. E. M.; Blomberg, M. R. A.; Svensson, M. *Chem. Phys. Lett.* **1994**, *223*, 35.
(25) Siegbahn, P. E. M.; Svensson, M.; Boussard, P. J. E. *J. Chem. Phys.* **1995**, *102*, 5377.
(26) Wittborn, A. M. C.; Costas, M; Blomberg, M. R. A.; Siegbahn, P. E. M. To be published.
(27) Holthausen, M. C.; Fiedler, A.; Schwarz, H.; Koch, W. *J. Phys. Chem.* **1996**, *100*, 6236.
(28) Holthausen, M. C.; Heinemann, C.; Cornell, H. H.; Koch, W.; Schwarz, H. *J. Chem. Phys.* **1995**, *102*, 4931.
(29) Blomberg, M. R. A.; Siegbahn, P. E. M.; Svensson, M. *J. Chem. Phys.* **1996**, *104*, 9546.
(30) Ricca, A.; Bauschlicher, C. W. *Chem. Phys. Lett.* **1995**, *245*, 150.
(31) Becke, A. D. *Phys. Rev.* **1988**, *A38*. 3098; Becke, A. D. *J. Chem. Phys.* **1993 98** 1372; Becke, A. D. *J. Chem. Phys.* **1993**, *98*, 5648.
(32) Perdew, J. P.; Wang, Y. *Phys. Rev. B* **1992**, *45*, 13244. Perdew, J. P. In *Electronic Structure of Solids*; Ziesche, P., Eischrig, H., Eds.; Akademie Verlag: Berlin, 1991. Perdew, J. P.; Chevary, J. A.; Vosko, S. H.; Jackson, K. A.; Pederson, M. R.; Singh, D. J.; Fiolhais, C. *Phys. Rev. B* **1992**, *46*, 6671.
(33) Eller, K.; Schwarz, H. *Int. J. Mass Spectrom. Ion Processes* **1989**, *93*, 243.
(34) Eller, K.; Zummack, W.; Schwarz, H. *J. Am. Chem. Soc.* **1990**, *112*, 621.
(35) Freiser, B. S. *Talanta* **1982**, *32*, 697.
(36) Freiser, B. S. *Anal. Chim. Acta* **1985**, *178*, 137.
(37) Forbes, R. A.; Laukien, F. H.; Wronka, J. *Int. J. Mass Spectrom. Ion Processes* **1988**, *83*, 23.
(38) Su, T.; Bowers, M. T. *Int. J. Mass Spectrom. Ion Phys.* **1973**, *12*, 347.
(39) Wittborn, C. A. M; Wahlgren, U. Private communication.
(40) Frisch, M. J.; Trucks, G. W.; Schlegel, H. B.; Gill, P. M. W.; Johnson, B. G.; Robb, M. A.; Cheeseman, J. R.; Keith, T.; Petersson, G. A.; Montgomery, J. A.; Raghavachari, K.; Al-Laham, M. A.; Zakrzewski, V. G.; Ortiz, J. V.; Foresman, J. B.; Cioslowski, J.; Stefanov, B. B.; Nanayakkara, A.; Challacombe, M.; Peng, C. Y.; Ayala, P. Y.; Chen, W.; Wong, M. W.; Andres, J. L.; Replogle, E. S.; Gomperts, R.; Martin, R. L.; Fox, D. J.; Binkley, J. S.; Defrees, D. J.; Baker, J.; Stewart, J. P.; Head-Gordon, M.; Gonzalez, C.; Pople, J. A.; *Gaussian 94, Revision B.2*; Gaussian Inc.: Pittsburgh, PA, 1995.
(41) Lee, C.; Yang, W.; Parr, R. G. *Phys. Rev.* **1988**, *B37*, 785.
(42) Vosko, S. H.; Wilk, L.; Nusair, M. *Can. J. Phys.* **1980**, *58*, 1200.
(43) Stevens, P. J.; Devlin, F. J.; Chablowski, C. F.; Frisch, M. J. *J. Phys Chem.* **1994**, *98*, 11623.
(44) Chong, D. P.; Langhoff, S. R. *J. Chem. Phys.* **1986**, *84*, 5606.
(45) Pople, J. A.; Head-Gordon, M.; Fox, D. J.; Raghavachari, K.; Curtiss, L. A. *J. Chem. Phys.* **1989**, *90*, 5622.
(46) STOCKHOLM is a general purpose quantum chemical set of programs written by P. E. M. Siegbahn, M. R. A. Blomberg, L. G. M. Pettersson, B. O. Roos, and J. Almlöf.
(47) Swang, O.; Faegri, Jr, K.; Gropen, O. *J. Phys. Chem.* **1994**, *98*, 3006.
(48) Huzinaga, S. *J. Chem. Phys.* **1965**, *42*, 1293.
(49) Hay, P. J.; Wadt, W. R. *J. Chem. Phys.* **1985**, *82*, 299.
(50) Stevens, W. J.; Krauss, M.; Basch, H.; Jasien, P. G. *Can. J. Chem.* **1992**, *70*, 612.
(51) Dunning, T. H. *J. Chem. Phys.* **1971**, *55*, 716.
(52) Heinemann, C.; Koch, W.; Schwarz, H. *Chem. Phys. Lett.* **1995**, *245*, 509.
(53) Koseki, S.; Gordon, M. S.; Schmidt, M. W.; Matsunaga, N. *J. Phys. Chem.* **1995**, *99*, 12764.
(54) Schmidt, M. W.; Baldridge, K. K.; Boatz, J. A.; Elbert, S. T.; Gordon, M. S.; Jensen, J. H.; Koseki, S.; Matsunaga, N.; Nguyen, K. A.; Su, S.; Windus, T. L.; Dupuis, M.; Montgomery, J. A. *J. Comput. Chem.* **1993**, *14*, 1347.
(55) See, for example: Landau, L. D.; E. Lifshitz, E. M. *Quantum Mechanics (Non-relativistic Theory)*; Pergamon Press: Oxford, 1958.
(56) Moore, C. E. *Atomic Energy Levels*; U.S. Department of Commerce, National Bureau of Standards, U.S. Government Printing Office: Washington, DC, 1952.
(57) Armentrout, P. B. Private communication.
(58) Bauschlicher, C. W., Jr.; Partridge, H. *J. Chem. Phys.* **1995**, *103*, 1788.
(59) Roos, B. O.; Taylor, P. R.; Siegbahn, P. E. M. *Chem. Phys.* **1980**, *48*, 157.
(60) Andersson, K.; Malmqvist, P. Å.; Roos, B. O.; Sadlej, A. J.; Wolinski, K. *J. Phys. Chem.* **1990**, *94*, 5483.
(61) Andersen, A.; Cordes, H.-G.; Herwig, J.; Kaminsky, W.; Merck, A.; Mottweiler, R.; Pein, J.; Sinn, H.; Vollmer, H.-J. *Angew. Chem.* **1976**, *88*, 689.